

Ultra-sharp pinnacles sculpted by natural convective dissolution

Jinzi Mac Huang^a, Joshua Tong^a, Michael Shelley^{a,b}, and Leif Ristroph^a

^aNew York University, Courant Institute, Applied Math Lab, 251 Mercer St, New York, NY USA 10012; ^bFlatiron Institute, Center for Computational Biology, 162 Fifth Avenue, New York, NY USA 10010

This manuscript was compiled on April 28, 2020

1 **The evolution of landscapes, landforms and other natural structures**
2 **involves highly interactive physical and chemical processes that of-**
3 **ten lead to intriguing shapes and recurring motifs. Particularly in-**
4 **tricate and fine-scale features characterize the so-called karst mor-**
5 **phologies formed by mineral dissolution into water. An archetypal**
6 **form is the tall, slender and sharply-tipped karst pinnacle or rock**
7 **spire that appears in multitudes in striking landforms called stone**
8 **forests, but whose formative mechanisms remain unclear due to**
9 **complex, fluctuating and incompletely understood developmental**
10 **conditions. Here we demonstrate that exceedingly sharp spires also**
11 **form under the far simpler conditions of a solid dissolving into a**
12 **surrounding liquid. Laboratory experiments on solidified sugars in**
13 **water show that needlelike pinnacles, as well as bed-of-nails-like ar-**
14 **rays of pinnacles, emerge robustly from the dissolution of solids with**
15 **smooth initial shapes. Although the liquid is initially quiescent and**
16 **no external flow is imposed, persistent flows are generated along the**
17 **solid boundary as dense, solute-laden fluid descends under grav-**
18 **ity. We use these observations to motivate a mathematical model**
19 **that links such boundary layer flows to the shape evolution of the**
20 **solid. Dissolution induces these natural convective flows that in turn**
21 **enhance dissolution rates, and simulations show that this feedback**
22 **drives the shape toward a finite-time singularity or blow-up of apex**
23 **curvature that is cut off once the pinnacle tip reaches microscales.**
24 **This autogenic mechanism produces ultra-fine structures as an at-**
25 **tracting state or natural consequence of the coupled processes at**
26 **work in the closed solid-fluid system.**

Geomorphology | Fluid-structure interaction | Dissolution | Natural convection | Stone forest

1 **T**he tall and pointed rock spires or pinnacles of Fig. 1 stand in
2 sharp contrast to the smoothed shapes and shallow slopes com-
3 monly associated with erosion and weathering. That pinnacles appear
4 in multitudes in vast arrays called stone forests (1, 2), and that such
5 landforms are found worldwide (3–7), suggests robust mechanisms
6 underlying their development. These structures are examples of karst
7 topographies that form by mineral dissolution in water (2, 8), but the
8 environmental and hydrological conditions essential to their forma-
9 tion are unclear. Geomorphological studies have detailed the rich
10 developmental histories of stone forests involving, among many other
11 complexities, periods of complete or partial submersion under water,
12 burial under loose sediment, and exposure to surface erosion (3–7, 9).
13 While superficial features such as channels and grooves seem linked
14 to rain runoff (2), it is unclear how much shape development occurred
15 prior to surface processes. Further, stone forests have been discovered
16 buried under loose sediment (10), suggesting that surface erosion is
17 not essential to the pinnacle motif. Mineral spires can result from
18 complete submersion under water followed by drainage (11), though
19 the degree of shape development during these stages is unclear. Given
20 the uncertainties regarding which factors are most critical, the study of
21 pinnacle formation may benefit from laboratory experiments in which

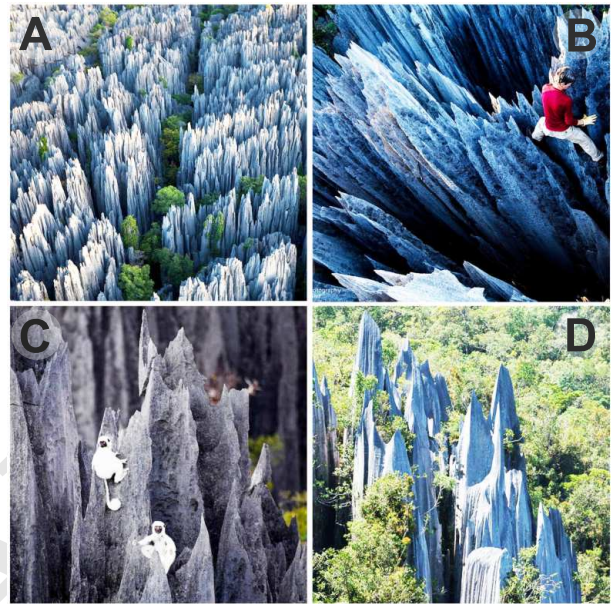


Fig. 1. Natural pinnacles and stone forests. (A)–(C) Photographs showing limestone structures of different scales in the Tsingy de Bemaraha National Park in Madagascar. Image credits to Steven Alvarez. (D) Similar limestone formations in the Gunung Mulu National Park of Malaysia. Image credit to Grant Dixon.

conditions can be imposed and cleanly controlled and the relevant shape developments observed and measured.

Viewed mathematically and physically, the action of erosion, dis-

Significance Statement

This work reveals a mechanism that may contribute to the formation of sharply pointed rock spires in karst or dissolved landforms such as stone forests. We show that solids dissolving into liquids in the presence of gravity naturally produce flows that carve ultra-sharp spikes. Better understanding the origin of these delicate structures may aid in natural conservation efforts. Our experimental and theoretical techniques may also be applied to other problems in geomorphology and phase-change processes such as ice melting. The mechanism could be used to manufacture fine-scale structures, and our theory provides the relevant control parameters.

J.M.H., J.T. and L.R. designed and conducted the experiments and analyzed the data; J.M.H. and M.S. designed the mathematical model and implemented simulations; all authors contributed to the interpretation of the results and to composing the manuscript.

The authors declare no conflicts of interest.

To whom correspondence should be addressed. Email: ristroph@cims.nyu.edu or shelley@cims.nyu.edu

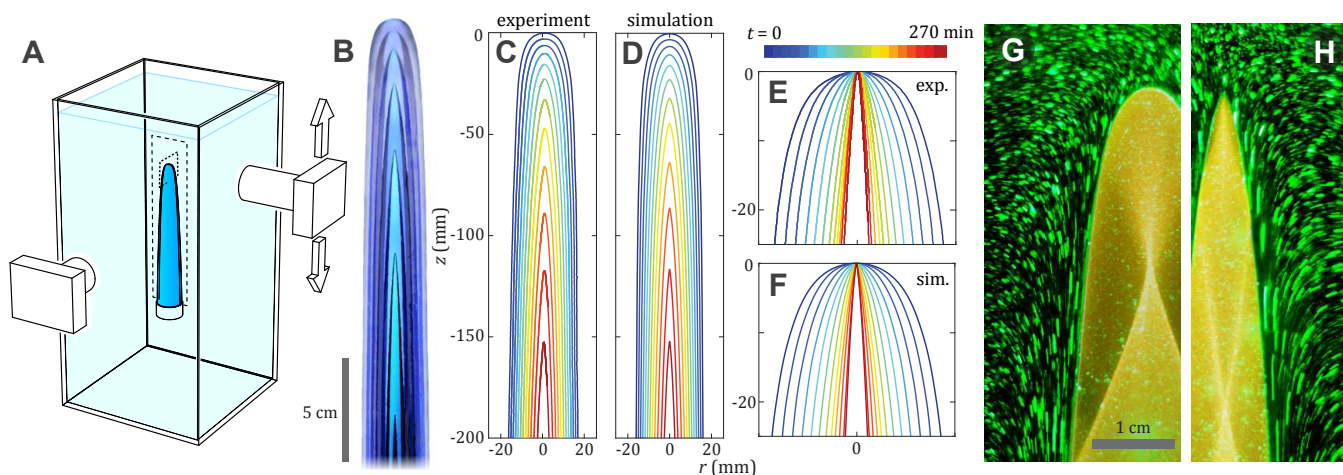


Fig. 2. Emergence of pinnacles in experiment and simulation. (A) Laboratory experiments. An upright object cast from solidified sugars dissolves in a large tank of water. One camera captures full-view images of the solid as it develops in time, and a second is zoomed-in and follows the apex region. (B) Overlaid full-view images spaced at an interval of 50 minutes. (C) Solid-liquid boundary profile extracted from full-view images and displayed every 25 minutes. (D) Corresponding boundary profiles as computed by the simulation. (E) and (F) Development of the apex region in experiment and simulation. These profiles are shown in the moving frame of the apex, revealing a trend towards sharper structures. (G) and (H) Flow visualization via streakline photography of microparticles illuminated by a laser sheet. Flows descend along the surface and entrain fluid from the sides at both early and later times.

25 solution or melting on stone, soil, sand, ice and other natural materials
 26 can be categorized as free- or moving-boundary problems (12, 13).
 27 This perspective is especially useful for understanding fundamental
 28 shape changing mechanisms and for disentangling the interdependent
 29 solid and fluid dynamics that arise when boundaries are carved
 30 by flowing air or water (14–16). The study of shape-flow interactions
 31 also benefits from laboratory experiments, which complement
 32 geomorphological field studies by permitting observation and measurement
 33 on tractable length and time scales and under controlled and
 34 reproducible conditions (17). Experiment and mechanistic theory,
 35 including mathematical modeling and simulation, have been usefully
 36 applied towards problems ranging from the growth and form of icicles
 37 (18) to landforms such as dunes (19), large-scale landscapes (20–22)
 38 and even global-scale flow-structure couplings such as continental
 39 drift driven by mantle convection (23, 24).

40 These past successes motivate the application of the moving-
 41 boundary approach to dissolution and towards understanding karst
 42 morphologies and pinnacles specifically. Here, we show experimentally
 43 and theoretically that ultra-sharp pinnacles emerge robustly as
 44 natural consequences of dissolution in the presence of gravity. Building
 45 on recent work (25–27), we conduct clean and controlled laboratory
 46 experiments aimed at understanding the minimal conditions needed to
 47 form pinnacles. Precision measurements allow for close comparison
 48 with a moving-boundary mathematical model that incorporates the
 49 relevant flow physics and chemistry of dissolution. Together these
 50 methods uncover a self-sculpting process by which the flows naturally
 51 generated during dissolution also reshape solids into microscopically-
 52 sharp spikes. Because it is at work under commonplace conditions,
 53 we speculate that this mechanism contributes to the formation of
 54 pinnacles in nature.

55 Laboratory experiments

56 To assess experimentally the development of a dissolving solid under
 57 idealized and controlled conditions, we consider objects made of
 58 solidified sugars cast into simple initial shapes and submerged into a
 59 large tank of water (Fig. 2A). The relatively high solubility of sugars
 60 in comparison to natural minerals allows for tractable run times of

hours. The initial form resembles an upright cylinder supported from
 below, and its apex is smooth and blunt. This starting shape can be
 viewed as analogous to the vertical columns formed between intersecting
 planar fissures that are thought to initiate pinnacle karst (3–7, 9). The
 choice of a tall column extends the dissolution process and allows for
 observation of the long-time shape dynamics. The object, which is
 observed to retain axisymmetry, is photographed over time by two
 cameras, one of which is fixed and captures the entire boundary and
 the other mounted to a moving stage to follow the apex and capture
 zoomed-in images. Additional experimental details are available in
 Materials and Methods and as Supplementary Information.

The overlaid images of Fig. 2B and the corresponding Supplementary
 Video 1 show a typical trial. The initially rounded column is seen to
 sharpen into a needlelike spire as the boundaries recede. Boundary
 profiles extracted from photographs are shown in Figs. 2C and E, the
 latter in the frame of the descending tip. Strikingly, these data indicate
 that the object becomes ever more slender and its tip ever sharper
 throughout the dissolution process. These observations are reproducible
 across trials and for different initial geometries, as supported by the
 extended data figures in the Supplementary Information.

A critical but unseen factor in these shape dynamics is the role of
 flow. Although the water is initially quiescent and no external flow is
 imposed throughout our experiments, the fluid is brought into motion
 by the dissolution process itself. To visualize these flows, we perform
 separate experiments in which we seed the water with microparticles
 and illuminate from above with planar laser light. As shown in Figs.
 2G and H, time-exposed photographs capture streaklines indicative of
 flows of speeds on the order of 1 cm/s that descend along the surface.
 This effect can be attributed to the fact that the solid is denser than
 the liquid and that flows are generated along the surface as the dense,
 solute-laden fluid descends under gravity.

A moving-interface model

Close inspection of the experimental shapes of Fig. 2B and C reveals
 that the pinnacle tip experiences higher dissolution rate than other
 locations on the surface, and yet the apex is not blunted but rather

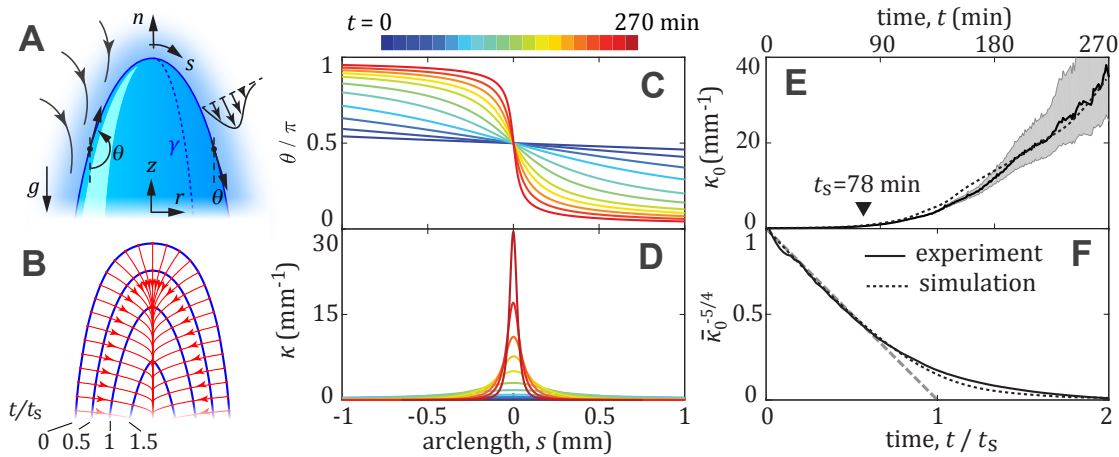


Fig. 3. Pinnacle formation as a geometric shock or curvature singularity. (A) Schematic defining the model and its variables. A solid of axisymmetric shape dissolves into surrounding liquid, and boundary layer flows are induced as dense, solute-laden fluid descends under gravity. (B) Shape evolution near the apex from simulation. The singularity or shock formation time t_s is associated with the intersection of characteristic curves (red). (C) Shape development as quantified by tangent angle θ versus arclength s . The approach to a step function is a signature of a geometric shock. (D) Shape development as quantified by curvature κ . The blow up of the apex curvature is a signature of a mathematical singularity. (E) Unbounded growth of apex curvature in experiment and simulation. The gray region represents error bars propagated based on the experimental resolution. (F) Power law behavior of curvature in the lead-up to the shock or singularity.

97 sharpens. Such paradoxes are best resolved by mathematical treatment
 98 as a free- or moving-boundary problem (12), in which the solid-
 99 liquid interface is viewed as a receding surface whose dynamics are
 100 dictated by the physics, chemistry and fluid dynamics of dissolving
 101 (28, 29). The natural convective flows observed in experiments are
 102 expected to play the important role of transporting solute along the
 103 surface. These flows thus modify the local solute concentration and
 104 the local dissolution rate, which Fick's law of diffusion dictates as
 105 proportional to the gradient in solute concentration normal to the
 106 surface (28). These effects are incorporated into a mathematical
 107 model using boundary layer theory (29), which describes the flow
 108 and concentration fields that vary strongly within a thin region of
 109 the fluid surrounding the solid. In this way, we arrive at an evolution
 110 equation for the interface in which the local normal velocity is related
 111 to the global shape. The dissolution rate is also subject to the Gibbs-
 112 Thomson effect, which acts to enhance dissolution rates in proportion
 113 to local curvature (30, 31). Complete model derivations as well as
 114 details of their numerical solution are given in Materials and Methods
 115 and as Supplementary Information.

116 Our model furnishes boundary dynamics in remarkable agreement
 117 with experiments, as shown in Figs. 2D and F and the Supplementary
 118 Video 2. Notably, we recover the observed tendency towards a sharp
 119 pinnacle, and this behavior is robust to initial shape and to model
 120 parameters (see Supplementary Information). Taken together, these
 121 results indicate that pinnacles emerge as the shape attractors for solids
 122 dissolving into fluids in the presence of gravity.

123 Pinnacle formation as a geometric shock & curvature 124 singularity

125 Further analysis of the shape dynamics in experiment and theory
 126 reveals a common approach to the formation of a sharp apex. The
 127 boundary shape can be represented by revolving a planar curve γ that
 128 is characterized by its tangent angle $\theta(s, t)$ as a function of arclength
 129 s and time t , as defined in Fig. 3A. As shown in the plot of Fig. 3C,
 130 curves of $\theta(s, t)$ over time for the simulations of Fig. 2 show an
 131 approach to an abrupt drop in the tangent angle, which is suggestive
 132 of a geometric shock (32). As shown in Fig. 3B, another signature
 133 of a shock can be seen in the converging characteristic curves that

represent trajectories of points propagated normally to the boundary
 (32). Further, local curvature is given by $\kappa(s, t) = -\partial\theta/\partial s$ and
 plotted in Fig. 3D, where unbounded growth of curvature quantifies
 the sharpening dynamics.

137 These observations are further elucidated by an analysis of our
 138 model equations showing that, if only hydrodynamic (boundary layer
 139 flows) but not thermodynamic (Gibbs-Thomson) effects are included,
 140 then the pinnacle evolves to infinite apex curvature $\kappa_0(t) = \kappa(s = 0, t)$
 141 in finite time. We derive a power law for this mathematical
 142 singularity as $\kappa_0(t) = \kappa_0(0)(1 - t/t_s)^{-4/5}$, where $\kappa_0(0)$ is the initial
 143 tip curvature and $t_s > 0$ is the time at which the singularity develops
 144 (see Supplementary Information). This analysis motivates a recasting
 145 of the curvature dynamics as $\bar{\kappa}_0(t)^{-5/4} = [\kappa_0(t)/\kappa_0(0)]^{-5/4}$, and
 146 indeed the experimental and model data of Fig. 3F follow the expected
 147 linear trend until late times.

148 In the later stages of dissolution, Fig. 3F shows that the curvature
 149 growth continues but at a nonsingular pace. This may be attributed to
 150 the Gibbs-Thomson effect, which strongly enhances the dissolution
 151 rate at the apex, blunting the tip and cutting off the singularity. In
 152 experiments, the radius of curvature of the tip eventually reaches tens
 153 of micrometers and approaches the imaging resolution of our system
 154 (see Materials and Methods and Supplementary Information). Theory
 155 predicts an ultimate fineness on the order of ten micrometers, a value
 156 set by material parameters.

158 Pinnacle forests from dissolution of porous solids

159 Returning to the motivating landforms of Fig. 1, we next ask how
 160 dissolution and the dissolutive sharpening mechanism described above
 161 might produce many spires in parallel. We hypothesize that the fluid-
 162 filled pores or fissures in a porous, soluble material serve as conduits
 163 for the flows produced during dissolution. Initially small, such cavities
 164 expand as their walls are consumed by the dissolving action and
 165 eventually merge or collide into one another. The interstitial solid
 166 regions may be shaped into pillars by the downward convective flows
 167 and then sharpened into pinnacles by the mechanism studied here.
 168 We experimentally test this picture in a highly idealized scenario of
 169 a soluble solid block seeded with an array of pores and immersed
 170 in liquid. Casting molten sugars in a mold containing thin wires,

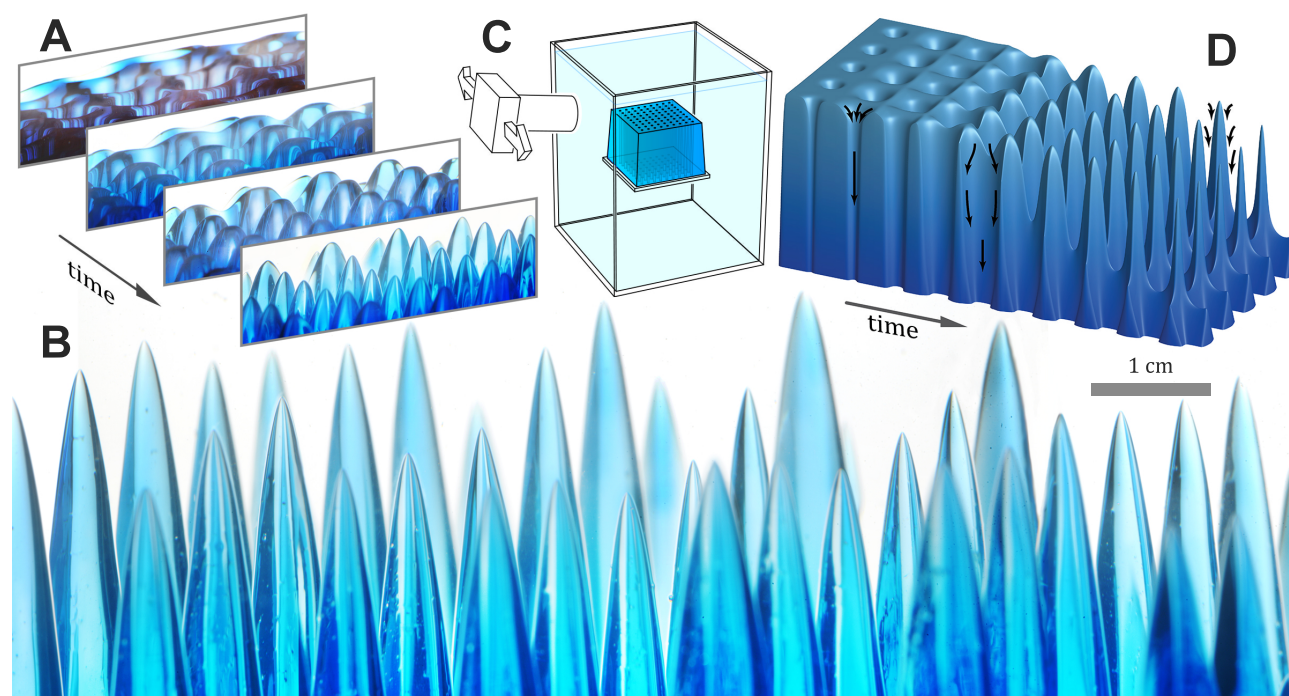


Fig. 4. Bed-of-nails morphology from dissolution of a porous solid. (A) Temporal progression of a dissolving block seeded with vertical pores. The openings widen and in their interstices develop into rounded hills, which then steepen into pillars. (B) The pillars sharpen to form an array of pinnacles. (C) Experimental schematic. A block of solidified sugar is cast with vertical pores and then immersed in water and imaged. (D) Interpretive schematic showing shape progression and expected flow structure.

171 which are removed after solidification, yields a large block spanned
 172 by vertical pores that are arranged in a square lattice (Materials and
 173 Methods). The block is supported on an elevated base and entirely
 174 submerged under water where it is photographed over time (Fig. 4C).
 175 The pores run the height of the block and base, allowing fluid to be
 176 conveyed downward during the dissolution process.

177 As shown in the photographs of Figs. 4A and B and Supplementary
 178 Video 3, the solid undergoes dramatic changes in shape as it
 179 dissolves. At early times, the openings of the pores on the upper
 180 surface widen, and the pores thus take on a fluted sectional profile,
 181 as shown schematically in Fig. 4D. This may be attributed to higher
 182 dissolution rates near the openings as fresh water from above is drawn
 183 downward by natural convective flows. As they widen further, each
 184 set of four neighboring pores in the square lattice begin to collide or
 185 merge near their tops, yielding soft hilltops in their interstices and thus
 186 a gently rolling landscape dotted with sinkholes. The hillslopes then
 187 steepen to form distinct pillars whose rounded tops later sharpen into
 188 spires. In this final stage, each pinnacle in the array may be thought
 189 to develop independently and by the mechanism studied here, as the
 190 flows responsible for sculpting are confined to thin boundary layers.
 191 These events yield a bed-of-nails morphology, here a square lattice of
 192 spikes that reflects the initial lattice of pores. More random seeding of
 193 pore locations is expected to generate disordered arrays of pinnacles
 194 of varying girth and height, which may more closely resemble natural
 195 pinnacles and stone forests.

196 Discussion and conclusions

197 The tendency towards sharp structures can be understood qualitatively
 198 by noting that the entrainment into the surface flows of fresh fluid
 199 from the sides (Figs. 2G and H) tends to thin the concentration
 200 boundary layer and thus enhance dissolution rates. This mechanism of
 201 dissolutive sharpening requires only the commonplace conditions of a

202 solid dissolving into liquid and the consequent density variations and
 203 natural convective flows. It relies on stably attached boundary layers,
 204 which can be expected of the upper surface of a solid if the solute-
 205 laden fluid is denser than the far-field fluid (29). Gravitationally stable
 206 boundary layers in an inverted situation can be expected for lower
 207 surfaces and low-density, upwardly-buoyant flows, as is expected
 208 for the underside of an iceberg melting in cold waters (17). More
 209 generally, one anticipates parallels between melting and dissolution,
 210 with temperature playing a role analogous to solute concentration (29).
 211 For both processes, our model framework is general and versatile
 212 enough to address further questions of shape dynamics.

213 The conditions studied here are purposefully idealized, permitting
 214 clear identification and clean characterization of dissolutive sharpen-
 215 ing, its chemophysical mechanism and mathematical structure. By
 216 showing that pinnacle-like shapes arise spontaneously in closed solid-
 217 fluid systems, under constant conditions, and without external forcing
 218 beyond that of gravity, this study reveals a minimal set of ingredients
 219 essential to the needle and bed-of-nails motifs. Our experimental
 220 pinnacles are carved by boundary layer flows generated by the dis-
 221 solution process itself, whereas in nature the responsible flows may
 222 include subsurface drainage and surface runoff (2, 4, 9, 11). Our
 223 pinnacle arrays form via dissolutive widening of pores, whose initial
 224 arrangement set the pattern of pinnacles, and a similar progression
 225 towards stone forests is thought to be initiated by vertical columns
 226 between intersecting fissures (3–7, 9). Ultimately, similar shapes are
 227 observed in both the synthetic and natural systems, the former being
 228 associated with an attractor of the shape dynamics that emerges as
 229 details of the initial form are lost in the approach to a singularity.

230 Future work might assess the robustness of pinnacle formation for
 231 differing environmental conditions through laboratory experiments,
 232 models and simulations of the type presented here. For example, the
 233 effect of precipitation and surface runoff could be isolated for study by
 234 subjecting a soluble body in air to misting with water droplets or some

235 other form of simulated rain (2). Corresponding theory should account
 236 for dissolution into thin-film flows. Pinnacle formation while buried
 237 under loose sediment could be tested using sand or other granular
 238 material saturated with water (11), a model or simulation of which
 239 should account for the Darcy flow conditions in the porous medium.
 240 In such scenarios, the hydrological conditions may be held constant as
 241 in our study, or subject to time variations, say by cyclic draining and
 242 immersion. Results from all such studies would help to tell the origin
 243 story of these striking landforms whose ultra-fine features require
 244 special conservation efforts (33–35).

245 Materials and Methods

247 **A. Materials and fabrication.** Objects made of solidified sugars are manu-
 248 factured by combining granulated table sugar, corn syrup and water in por-
 249 tion 8 : 3 : 2 by volume. The mixture is stirred continuously and brought
 250 to 150°C, at which point it is abruptly taken off the heat. The molten sugars
 251 are immediately poured into custom-shaped molds and allowed to gradually
 252 set over 12 hours or longer, which permits bubbles to rise out. This recipe
 253 achieves so-called hard crack candy, which is an amorphous solid of about
 254 99% sugar content. Cylindrical molds of about 25 cm height and diameters
 255 between 2 cm and 6 cm are used to make the pillars in the single pinnacle
 256 experiments. Once removed from the mold, the solid cylinder is reshaped
 257 on a spinning stage by dissolving with warm water applied with a sponge.
 258 This gives an initial form that is axisymmetric with a rounded top and slightly
 259 tapered sides. A cubic mold measuring 10 × 10 × 10 cm in length, width
 260 and height is used for the pinnacle array experiments. The bottom of the mold
 261 receives metal rods of diameter 0.4 cm that stand upright in a square 7-by-7
 262 array of spacing 1.3 cm. After casting, the rods are removed to leave an array
 263 of pores that vertically span the block.

264 **B. Dissolution experiments and image acquisition.** The experiments
 265 are conducted in a clear acrylic (plexiglass) tank measuring 30 × 30 × 60 cm in
 266 length, width and height that is filled with degassed water at room temperature
 267 of 23 ± 1°C. The depth of the tank allows the dense fluid containing dissolved
 268 sugars to settle at the bottom and far from the test object. Image acquisition
 269 is accomplished by two synchronized Nikon D610 digital cameras capturing
 270 photographs at 1 minute intervals and directed normally to two adjacent side
 271 walls. Each is back lit with cold LED lights shone on a diffusive screen. On
 272 the screen and on either side the object are opaque sheets whose refraction
 273 through the object cause the boundary to appear dark on the light background.
 274 The zoomed-out camera is fixed in position and captures the overall shape of
 275 the dissolving object with resolution 11.3 pixels/mm. The zoomed-in camera
 276 is fitted with a macro lens and captures images around the apex at resolution
 277 173 pixels/mm. For the single pinnacle experiments, this camera is mounted
 278 on a vertical translation stage so that the apex may be maintained in the center
 279 of view throughout the experiment. For the pinnacle array experiments, the
 280 zoomed-in camera is mounted on a horizontal stage and panned across the
 281 upper surface as several photographs are taken. These images are later digitally
 282 registered and combined.

283 **C. Image processing and profile extraction.** For the single pinnacles, the
 284 contour of the interface is extracted via a custom-written MATLAB code using
 285 the Image Processing Toolbox. For the zoomed-in images, the contour near the
 286 apex is fit to a 4th order polynomial, and the spatial distribution of the tangent
 287 angle $\theta(s, t)$ and the apex curvature $\kappa_0(t)$ are then computed from the fit.

288 **D. Boundary layer theory model and shock formation.** The solid-
 289 liquid interface recedes with velocity proportional to the normal gra-
 290 dient of concentration, $V_n \sim \mathbf{n} \cdot \nabla c$, where the prefactor may
 291 be calculated from conservation of mass and Fick’s law of diffusion.
 292 The concentration field c and its gradient at the interface are ob-
 293 tained from boundary layer theory, yielding the expression $V_n(s, t) =$
 294 $-a[r(s, t) \cos \theta(s, t)]^{1/3} / [\int_0^s r(s', t)^{4/3} \cos^{1/3} \theta(s', t) ds']^{1/4}$ for the local
 295 dissolution rate as a function of the shape, expressed here as the tangent
 296 angle $\theta(s, t)$ at each location s and time t . Here, the constant $a \sim 10^{-7}$
 297 $\text{m}^{5/4}/\text{s}$ is estimated from material properties in experiment. The axisymmetric
 298 geometry of the dissolving object is characterized by revolving a planar curve
 299 γ around the z -axis, as shown in Fig. 3a. The evolution of γ is then prescribed
 300 by $\partial_t \theta - V_s \partial_s \theta = \partial_s V_n$. The prescription of a tangential velocity V_s does

not change the shape but is imposed in order to preserve the spacing in ar-
 clength so that s and t remain independent variables. The s -derivative of the θ
 equation in the limit as $s \rightarrow 0$ leads to an ordinary differential equation for
 the apex curvature, $d\kappa_0/dt = -\partial_s^2 V_n(0, t) - V_n(0, t)\kappa_0^2 \sim \kappa_0^{9/4}$, whose
 solution diverges in finite time.

E. Gibbs-Thomson effect. The Gibbs-Thomson effect describes the effect
 of curvature on the saturation concentration at a solid-liquid interface: $c_s^* =$
 $c_s \exp(\epsilon \hat{\kappa})$ for a surface of mean curvature $\hat{\kappa}$, where c_s is associated with a
 flat interface ($\hat{\kappa} = 0$). Here $\epsilon \approx 10 \mu\text{m}$ is a material parameter estimated for
 our experimental conditions. As compared to a flat interface of dissolution rate
 V_n , a curved surface has enhanced saturated concentration and thus enhanced
 dissolution rate of the form $V_n^* = V_n(1 + \epsilon \hat{\kappa})$. In the θ dynamical equation,
 this effect manifests as a diffusion term that suppresses high curvature by
 enhancing dissolution rate. At the apex, the two principal curvatures are
 identical and thus $\hat{\kappa}(0, t) = \kappa_0(t)$, and the Gibbs-Thomson effect becomes
 significant when $1/\kappa_0 \approx \epsilon \approx 10 \mu\text{m}$.

F. Simulation method and implementation. A custom written numerical
 scheme employs the $\theta - L$ method to solve dynamical equations for the tangent
 angle θ and total arclength L (36). The numerical simulations are performed in
 MATLAB with second order finite differences in space. In time, a second order
 Adam-Bashforth backward differentiation method mitigates the stiffness and
 nonlinearity of the equations. Consistent parameter values of $a = 4.5 \times 10^{-7}$
 $\text{m}^{5/4}/\text{s}$ and $\epsilon = 11 \mu\text{m}$ are used throughout all examples in this Article and
 the Extended Data Figures. These values are set by matching the evolution of
 tip curvature κ_0 and the total arclength L for the experiment in Figs. 2 and 3,
 and the resulting choice leads to excellent agreement across all experiments.

ACKNOWLEDGMENTS. We thank M. Davies Wykes, S. Childress
 and J. Zhang for useful discussions and the National Science Foundation for
 support (NSF CBET-1805506).

1. Marjorie M Sweeting. *Karst in China: Its Geomorphology and Environment*. Springer Verlag Berlin-Heidelberg, 1995.
2. Angel Ginés, Martin Knez, Tadej Slabe, and Wolfgang Dreybrodt. *Karst Rock Features: Karren Sculpturing*. Založba ZRC, 2009.
3. RG Ley. The pinnacles of Gunung Api. *Geographical Journal*, 146:14–21, 1980.
4. Lin Hua Song. Origination of stone forests in China. *International Journal of Speleology*, 15(1):1, 1986.
5. Márton Veress, Dénes Lóczy, Zoltán Zentai, Gábor Tóth, and Roland Schläffer. The origin of the Bemaraha tsingy (Madagascar). *International Journal of Speleology*, 37(2):6, 2008.
6. Márton Veress, Gabor Toth, Zoltan Zentai, and Roland Schläffer. The Ankarana tsingy and its development. *Carpethian Journal of Earth and Environmental Sciences*, 4(1):95–108, 2009.
7. Márton Veress, Zoltán Zentai, Kálmán Péntek, Ljubov Döbrönte, and Ljubov Danilovna Kipriyanova. The development of the pinnacles (Lena pillars) along Middle Lena (Sakha Republic, Siberia, Russia). *Proceedings of the Geologists’ Association*, 125(4):452–462, 2014.
8. Derek Ford and Paul D Williams. *Karst Hydrogeology and Geomorphology*. John Wiley & Sons, 2013.
9. Peng Jian, Cai Yunlong, Yang Minde, Liang Hong, Liang Fuyuan, and Song Linhua. Relating aerial erosion, soil erosion and sub-soil erosion to the evolution of Lunan Stone Forest, China. *Earth Surface Processes and Landforms*, 32(2):260–268, 2007.
10. Martin Knez, Bojan Otoničar, and Tadej Slabe. Subcutaneous stone forest (Trebnje, central Slovenia). *Acta Carsologica*, 32(1), 2003.
11. Tadej Slabe, Asami Hada, and Martin Knez. Laboratory modeling of karst phenomena and their rock relief on plaster: Subsoil karren, rain flutes karren and caves. *Acta Carsologica*, 45(2), 2016.
12. John Crank. *Free and Moving Boundary Problems*. Clarendon Press Oxford, 1984.
13. Leif Ristroph. Sculpting with flow. *Journal of Fluid Mechanics*, 838:1–4, 2018.
14. Leif Ristroph, Matthew NJ Moore, Stephen Childress, Michael J Shelley, and Jun Zhang. Sculpting of an erodible body by flowing water. *Proceedings of the National Academy of Sciences*, 109(48):19606–19609, 2012.
15. Matthew NJ Moore, Leif Ristroph, Stephen Childress, Jun Zhang, and Michael J Shelley. Self-similar evolution of a body eroding in a fluid flow. *Physics of Fluids*, 25(11):116602, 2013.
16. Khunsa Amin, Jinzi Mac Huang, Kevin J Hu, Jun Zhang, and Leif Ristroph. The role of shape-dependent flight stability in the origin of oriented meteorites. *Proceedings of the National Academy of Sciences*, 116(33):16180–16185, 2019.
17. Herbert E Huppert. The physical processes involved in the melting of icebergs. *Annals of Glaciology*, 1:97–101, 1980.
18. Martin B Short, James C Baygents, and Raymond E Goldstein. A free-boundary theory for the shape of the ideal dripping icicle. *Physics of Fluids*, 18(8):083101, 2006.
19. Pascal Hersen, Stéphane Douady, and Bruno Andreotti. Relevant length scale of barchan dunes. *Physical Review Letters*, 89(26):264301, 2002.
20. Hans-Henrik Stølum. River meandering as a self-organization process. *Science*, 271(5256):1710–1713, 1996.
21. J Taylor Perron, James W Kirchner, and William E Dietrich. Formation of evenly spaced ridges and valleys. *Nature*, 460(7254):502, 2009.

- 374 22. Sean D Willett, Scott W McCoy, J Taylor Perron, Liran Goren, and Chia-Yu Chen. Dynamic
375 reorganization of river basins. *Science*, 343(6175):1248765, 2014.
- 376 23. Michael Gurnis. Large-scale mantle convection and the aggregation and dispersal of super-
377 continents. *Nature*, 332(6166):695, 1988.
- 378 24. Jun Zhang and Albert Libchaber. Periodic boundary motion in thermal turbulence. *Physical*
379 *Review Letters*, 84(19):4361, 2000.
- 380 25. Elias Nakouzi, Raymond E Goldstein, and Oliver Steinbock. Do dissolving objects converge
381 to a universal shape? *Langmuir*, 31(14):4145–4150, 2014.
- 382 26. Jinzi Mac Huang, M Nicholas J Moore, and Leif Ristroph. Shape dynamics and scaling laws
383 for a body dissolving in fluid flow. *Journal of Fluid Mechanics*, 765, 2015.
- 384 27. Megan S Davies Wykes, Jinzi Mac Huang, George A Hajjar, and Leif Ristroph. Self-sculpting
385 of a dissolvable body due to gravitational convection. *Physical Review Fluids*, 3(4):043801,
386 2018.
- 387 28. Veniamin G. Levich. *Physicochemical Hydrodynamics*. Prentice-Hall Inc., 1962.
- 388 29. Hermann Schlichting and Klaus Gersten. *Boundary-Layer Theory*. Springer, 2016.
- 389 30. HB Aaron and GR Kötler. The effects of curvature on the dissolution kinetics of spherical
390 precipitates. *Metal Science Journal*, 4(1):222–225, 1970.
- 391 31. Michel Perez. Gibbs-Thomson effects in phase transformations. *Scripta Materialia*, 52(8):
392 709–712, 2005.
- 393 32. L.C. Evans. *Partial Differential Equations*. Graduate Studies in Mathematics. American Math-
394 ematical Society, 2010.
- 395 33. Elery Hamilton-Smith. Karst and world heritage status. *Acta Carsologica*, 36(2), 2007.
- 396 34. Tsilavo Raharimahefa. Geoconservation and geodiversity for sustainable development in
397 madagascar. *Madagascar Conservation & Development*, 7(3):126–134, 2012.
- 398 35. Chuanrong Zhang, Michael Day, and Weidong Li. Landuse and land cover change in the
399 lunan stone forest, china. *Acta Carsologica*, 32(2), 2016.
- 400 36. Thomas Y Hou, John S Lowengrub, and Michael J Shelley. Removing the stiffness from
401 interfacial flows with surface tension. *Journal of Computational Physics*, 114(2):312–338,
402 1994.

DRAFT